Pergamon

Int. J. Solids Structures Vol. 34, No. 17, pp. 2161–2181, 1997
© 1997 Elsevier Science Ltd. All rights reserved
Printed in Great Britain
0020–7683/97 $17.00 + .00

PII: S0020–7683(96)00025–X

VIBRATION OF THERMOMECHANICALLY LOADED FLAT AND CURVED PANELS TAKING INTO ACCOUNT GEOMETRIC IMPERFECTIONS AND TANGENTIAL EDGE RESTRAINTS

LIVIU LIBRESCU and WEIQING LIN
Virginia Polytechnic Institute and State University, Engineering Science and Mechanics Department, Blacksburg, Virginia 24061-0219, U.S.A.

(*Received* 15 *September* 1995; *in revised form* 31 *January* 1996)

Abstract—A study of the effects played by tangential edge constraints on the vibrational behavior of single/multilayered doubly-curved shallow panels subjected to complex thermomechanical loading systems acting in the pre/postbuckling regimes is presented. In addition, effects related to the transverse shear and initial geometric imperfections are incorporated and their influence is highlighted. Numerical illustrations based on a higher-order theory underline the strong influence played by the above mentioned effects, in general, and by tangential-edge restrains on the alleviation of the intensity of the snap-through buckling, its delay and suppression, in particular. © 1997 Elsevier Science Ltd.

NOMENCLATURE

$a_{\alpha\beta}$, $a^{\alpha\beta}$	Covariant and contravariant components of the metric tensor of the undeformed mid-surface σ
A, B, C, S; b, c, $\tilde{b}$, $\tilde{c}$	Stiffness quantities (see Appendix)
$b_{\alpha\beta}$	Curvature tensor of the undeformed mid-surface
$b_{11}(\equiv 1/R)$; $b_{22}(\equiv 1/R_2)$	Principal curvatures of σ
D	Flexural stiffness (see Appendix)
c_1, c_2	Average tangential stiffness quantities in the direction normal to edge $x = 0$, l_1 and $x_2 = 0$, l_2, respectively
$e_{\alpha\beta}$, $e_{\alpha 3}$	Tangential and transverse shear 3-D strain components
E, E'	Young's modulus, tangential and transversal to the isotropy surface, respectively
F	Airy's potential function
G, G'	Tangential and transverse shear modulus
h	Thickness of shell/plate
H	Mean curvature of σ
K^2	Transverse shear correction factor
N_{11}, N_{22}	Edge loads normal to the edges $x_1 = 0$, l_1 and $x_2 = 0$, l_2, respectively, positive in compression
l_1, l_2	Length and width of the flat/curved panel
$\tilde{L}_{11}$, $\tilde{L}_{22}$	Dimensionless compressive edge loads $(\equiv (N_{11}, N_{22})l_1^2/\pi_D^4)$
$L^{\alpha\beta}$, $M^{\alpha\beta}$, $Q^{\alpha 3}$	Tensors of stress resultants, stress couples and transverse shear stress resultant, respectively
m_0	Mass per unit area of the laminated plate/shell
p_3, p_{mn}, $\hat{p}(\equiv p_{11}l_1^4/Eh^4)$	Lateral pressure field, its amplitude in the mode (m, n), and the dimensionless amplitude in the mode (1, 1), respectively
s^{ij}	Second Piola–Kirchhoff stress tensor
$\overset{0}{T}(x_\alpha)$, $\overset{1}{T}(x_\alpha)$	Uniform and non-uniform through thickness temperature distributions
$\overset{0}{T}_{mn}$, $\overset{1}{T}_{mn}$	Amplitudes in the mode (m, n) of $\overset{0}{T}$ and $\overset{1}{T}$, respectively
$\overset{0}{T}(\equiv \overset{0}{T}_{11})$, $\overset{0}{T}(\equiv \overset{1}{T}_{11})$	Notations used in numerical illustrations to denote the amplitudes in the mode (1, 1) of temperature distributions $\overset{0}{T}$ and $\overset{1}{T}$, respectively
$T_e(x_\alpha)$, $T_i(x_\alpha)$	The temperature distributions over the external and internal bounding surfaces of the plate/shell, respectively
T_e, T_i	The temperature amplitudes in mode (1, 1) of temperature distribution over the external and internal shell/plate surfaces
t	Time
v_α, v_3	Tangential and transversal displacement quantities of the mid-surface of plate/shell
w_{mn}	The amplitudes in the mode (m, n) of v_3
$\overset{0}{v}_3$	Initial geometric imperfection
$\overset{0}{w}_{mn}$	The amplitude in the mode (m, n) of $\overset{0}{v}_3$

x^i	Curvilinear system of normal coordinates
λ, λ'	Thermal compliance coefficients in the tangential and transversal directions to the isotropy surface, respectively
λ_1, λ_2	Tangential stiffness quantities in the direction normal to the edges $x_1 = 0$, l_1 and $x_2 = 0$, l_2, respectively
λ_m, μ_n	$m\pi/l_1$, $n\pi/l_2$
Λ, Π	Stretching and bending thermal stiffness quantities of plate/shell, respectively
δ_4	Tracer identifying the contribution brought by transverse normal stress
δ_H	Tracer identifying the contribution brought by higher-order terms
$\delta(\equiv w_{11}/h)$ $\delta_0(\equiv \overset{0}{w}_{11}/h)$	The dimensionless amplitudes of the transverse deflection and initial geometric imperfection, respectively
Δ	Two-dimensional Laplace operator in a curvilinear coordinate system $(\equiv (\cdot)\vert^{x}_{x})$
Δ_1	The end-shortening in the x_1 direction
ν, ν'	Poisson's ratios tangential and transversal to the isotropy surface
$\varepsilon_{\alpha\beta}$, $\kappa_{\alpha\beta}$, $\zeta_{\alpha\beta}$, $\varepsilon_{\alpha 3}$ and $\lambda_{\alpha 3}$	2-D strain measures
ϕ	Function associated with transverse shear
$(),_i$	Partial differentiation with respect to coordinates x^i
$()\vert_{i}$, $()\vert_{\alpha}$	Covariant differentiation with respect to the metric tensor g_{ij} and $a_{\alpha\beta}$, respectively
$\dot{()}$	Time derivative.

1. INTRODUCTION

The dynamic response and vibration behavior of mechanically and thermally loaded flat and curved panels is a problem of a special relevance in the design and development of supersonic/hypersonic vehicles as well as of future reusable space transportation systems.

During their missions, advanced flight vehicles have to withstand severe aerodynamic, aeroacoustic and thermomechanical loads. The temperatures are likely to range from the extreme lows of cryogenic fuels and radiation to space, to the highs associated with aerodynamic heating, heat from propulsion unit and radiation from the sun.

All these factors affect dramatically the dynamic response characteristics, aeroelastic behavior and fatigue life of these structures. In order to evaluate properly their dynamic performances, a better understanding of the effects played by non-uniform temperature fields and mechanical loading upon the vibrational behavior of aeronautical structures is needed.

Major portions of aircraft and spacecraft structures consist of plates and shells. In order to resist such adverse conditions, their structure is likely to be constructed of advanced composite materials.

In two recent papers (Librescu *et al.*, 1993b; 1994) the effects of transverse shear featured by the advanced composite materials and of initial geometric imperfections on natural frequencies of flat and curved panels subjected to thermomechanical load systems have been investigated. In these studies the panels have been considered simply-supported and it was assumed that the tangential motion in the direction normal to the unloaded edges is either unrestrained (free movable edges) or fully restrained (immovable edges). However, in practical situations, the tangential motion of the unloaded edges is *partially restrained* only.

As it was shown quite recently (Librescu *et al.*, 1994b, 1995), in the static case, the degree of the tangential edge restraint can play a great role in improving the load carrying capacity of structures by preventing the loss of their stability through a snap-through or via a bifurcational buckling with unstable postbuckling response. Moreover, it can render an imperfection-sensitive panel, insensitive to imperfection. Needless to say, the degree of the tangential edge restraint can play also an opposite effect upon the postbuckling behavior of mechanically and thermally loaded panels.

Related to the *vibrational behavior* of flat and curved panels subjected to thermomechanical loadings, the degree of the tangential restraint of panel edges is likely to play a significant influence, as well, upon the associated frequency-load interaction behavior. As a result, the present study has as one of its purposes the elucidation of the influence played by the tangential edge constraints on the natural frequencies of geometrically perfect and imperfect flat and curved panels subjected to complex thermal and mechanical loading conditions.

To the end of studying this problem and for rendering the paper reasonably self-contained the basic steps yielding the associated governing equation system will be presented. For more details the reader is referred to the papers by Librescu *et al.* (1993a,b,c). The analysis is carried out within a higher order shell theory developed within the Lagrangian description and in the spirit of the von Kármán's small strain and moderately small rotation concept.

In many instances, the numerical illustrations are displayed in parallel with their static counterpart. This enables one to get a better understanding on the influence played by the degree of tangential edge constraints, the non-uniform temperature and pressure fields, stress-free initial geometric imperfections, shell curvature, and transverse shear upon frequency-load interaction behavior.

2. GEOMETRICAL PRELIMINARIES. ASSUMPTIONS

Consider the case of doubly-curved shallow panels of uniform thickness h. Assume that the structure is symmetrically laminated of $2m+1$ ($m = 1, 2, \ldots$) elastic layers whose materials exhibit transversely isotropic thermo-elastic properties, the surface of isotropy being parallel at each point to the reference surface of the panel. It is supposed that the layers are in perfect bond so that no slip between the contiguous layers may occur.

The points of the 3-D space of the panel are referred to a set of curvilinear system of normal coordinates, x^i, where x^α ($\alpha = 1, 2$) and x^3 denote the tangential and transverse coordinate to the mid-surface, respectively, where the reference surface σ (coinciding with the mid-surface of the mid-layer) is defined by $x^3 = 0$.

In the forthcoming developments, the conditions pertinent to the theory of shallow shells (SST) are invoked. Denoting by $Z(\equiv Z(x^\alpha))$ the amount of deviation of the shell reference surface from its projection to a plane P, it is assumed that this quantity is small when compared with a maximum length of an edge of the shell or with the minimum radius of curvature of σ. Postulating that $\max(\partial Z/\partial x^\alpha) \ll 1$, it results (see, e.g., Green and Zerna, 1968) that the metric tensors associated with the system of coordinates on the plane σ and with its projection on P are the same and, in addition, that the curvature tensor of the reference surface behaves as a constant in the differentiation operation.

Having in view the intricacy of the resulting equations, in the following developments the tensorial notation will be used. In addition to their compactness, the invariance to any change of the reference frame constitutes another feature whose advantages have not to be advocated.

In the forthcoming developments, unless stated otherwise, the Einsteinian summation convention for the repeated indices is implied, where the Latin indices range from 1 to 3 while the Greek indices range from 1 to 2.

3. THERMOELASTIC CONSTITUTIVE EQUATIONS

As in the 3-D elasticity theory, it can be stated that the 3-D thermoelasticity theory implying small strains and large displacement gradients may be described by linear constitutive equations, correlating second Piola–Kirchhoff stress and Lagrangian strain tensor components. As a result, in the absence of stresses in the undeformed body, the stress–strain-temperature relationship for an elastically linear 3-D anisotropic body is given by the Duhamel–Neumann form of Hooke's law. Under a convenient form they can be expressed as (Librescu, 1975):

$$s^{\alpha\beta} = \tilde{E}^{\alpha\beta\omega\rho} e_{\omega\rho} + \delta_A \frac{E^{\alpha\beta 33}}{E^{3333}} s^{33} + \tilde{\lambda}^{\alpha\beta} T,$$

$$s^{\alpha 3} = 2E^{\alpha 3\omega 3} e_{\omega 3}. \tag{1a,b}$$

In these equations

$$\tilde{E}^{\alpha\beta\omega\rho} = E^{\alpha\beta\omega\rho} - \frac{E^{\alpha\beta 33}E^{33\omega\rho}}{E^{3333}}, \quad \tilde{\lambda}^{\alpha\beta} = \lambda^{\alpha\beta} - \frac{E^{\alpha\beta 33}}{E^{3333}}\lambda^{33}, \tag{2a,b}$$

denote the reduced elastic and thermal compliance coefficients, respectively (assumed to be independent of temperature), $T(\equiv T(x^{\omega}, x^3))$ denotes the temperature rise from a reference temperature T_r (at which the body does not undergo thermal expansions), while s^{ij} and e_{ij} stand for the second Piola–Kirchhoff stress and the Lagrangian strain tensors, respectively, δ_A being a tracing quantity identifying the contribution of s^{33} in the constitutive equations. For transversely-isotropic materials, the thermo-elastic moduli are expressed by

$$\tilde{E}^{\alpha\beta\omega\rho} = \frac{E}{1+\nu}\left[\frac{1}{2}(a^{\alpha\omega}a^{\beta\rho} + a^{\alpha\beta}a^{\alpha\rho}) + \frac{\nu}{1-\nu}a^{\omega\rho}a^{\alpha\beta}\right],$$

$$E^{\alpha 3\omega 3} = G' a^{\alpha\omega}; \quad \frac{E^{\alpha\beta 33}}{E^{3333}} = \frac{\nu' E}{E'(1-\nu)}a^{\alpha\beta},$$

$$\tilde{\lambda}^{\alpha\beta} = \tilde{\lambda}a^{\alpha\beta} \equiv \lambda\mathscr{A}a^{\alpha\beta}, \tag{3a–d}$$

where

$$\mathscr{A} = 1 - \frac{E\nu'}{E'(1-\nu)}\frac{\lambda'}{\lambda}. \tag{3e}$$

In eqns (3), E, ν, $G(\equiv E/2(1+\nu))$, λ and E', ν', G' and λ' denote Young's modulus, Poisson's ratio, shear modulus and the thermal compliance coefficient characterizing the material behavior tangent to the surface of isotropy and across this surface, respectively.

Consideration of this type of anisotropy is motivated by the following factors: (a) it enables one to emphasize in a more comprehensive way the effect played by transverse shear flexibility, (b) the materials exhibiting this kind of anisotropy (e.g., the pyrolitic graphite and the new products of alloys of pyrolitic graphite) play a great role in the thermal protection of aerospace vehicles and of engine nozzles (e.g., see (Garber, 1963 and Woods, 1976), and (c) such transversely-isotropic materials are used to model the core-layer of sandwich constructions.

Within the framework of this study a linear variation of the thermal field across the wall thickness is postulated, namely

$$T(x_{\alpha}, x_3) = \overset{0}{T}(x_{\omega}) + x_3\overset{1}{T}(x_{\omega}),$$

where

$$\overset{0}{T}(x^{\omega}) = \frac{1}{2}(T_i + T_e); \quad \overset{1}{T}(x^{\omega}) = \frac{1}{h}(T_i - T_e), \tag{4a–c}$$

define the membrane and the thickness-wise temperatures, respectively.

In eqns (4), $T_i(x^{\omega})(\equiv T(x^{\omega}, x_3 = h/2))$ and $T_e(x^{\omega})(\equiv T(x^{\omega}, x_3 = -h/2))$ are the temperature distributions over the bounding surfaces of the shell. From eqns (4), one obtains the relationships $h\overset{1}{T} = 2(\overset{0}{T} - T_e)$ and $h\overset{1}{T} = 2(T_i - \overset{0}{T})$ to be used in computations, in the cases when T_e and T_i are the temperatures whose amplitudes are hold fixed, respectively. $\overset{0}{T}$ and $\overset{1}{T}$ appear explicitly in the 2-D form of the constitutive equations and later, in the governing equations.

4. KINEMATIC EQUATIONS

Within the Lagrangian description and in the spirit of small strains and moderately small rotation approximation, the 3-D strain–displacement relationship is

$$2e_{ij} = V_{i|j} + V_{j|i} + V_{3|i}V_{3||j} + \overset{0}{V}_{3|i}V_{3|j} + V_{3||i}\overset{0}{V}_{3||j}, \tag{5}$$

where $V_i(x^\alpha, x^3, t)$ denote the displacement components while $\overset{0}{V}_3(x^\alpha, x^3) \equiv \overset{0}{v}_3(x^\alpha)$ denotes the initial geometric imperfection in the unstressed configuration. By convention, the transverse deflection is measured from the imperfect surface and is considered positive in the inward direction.

Assuming a parabolic variation for the shifted tangential displacement components through the entire thickness of the structure (see Reddy and Liu, 1987, Librescu and Stein, 1991), enforcing the conditions expressing the absence of shear tractions on the shell bounding surfaces, and using in eqn (5) the relationships between the covariant derivatives in the 3-D space with the ones in the 2-D (see Naghdi, 1963, and Librescu, 1975) in the light of the assumptions proper to the SST, one derive the nonvanishing components of the strain tensor as

$$e_{\alpha\beta} = \varepsilon_{\alpha\beta} + x^3\kappa_{\alpha\beta} + (x^3)^3\zeta_{\alpha\beta},$$
$$e_{\alpha 3} = \varepsilon_{\alpha 3} + (x^3)^2\lambda_{\alpha 3}. \tag{6a,b}$$

In eqn (6) the various 2-D strain measures are defined as

$$2\varepsilon_{\alpha\beta} = v_{\alpha|\beta} + v_{\beta|\alpha} - 2b_{\alpha\beta}v_3 + v_{3,\alpha}v_{3,\beta} + v_{3,\alpha}\overset{0}{v}_{3,\beta} + \overset{0}{v}_{3,\alpha}v_{3,\beta},$$
$$2\kappa_{\alpha\beta} = \psi_{\alpha|\beta} + \psi_{\beta|\alpha},$$
$$2\zeta_{\alpha\beta} = -\delta_H\frac{4}{3h^2}(2v_{3|\alpha\beta} + \psi_{\alpha|\beta} + \psi_{\beta|\alpha}),$$
$$2\varepsilon_{\alpha 3} = \psi_\alpha + v_{3,\alpha} + b^\rho_\alpha v_\rho,$$
$$2\lambda_{\alpha 3} = -\delta_H\frac{4}{3h^2}(\psi_\alpha + v_{3,\alpha} + b^\rho_\alpha v_\rho). \tag{7a–e}$$

Herein δ_H is a tracer identifying the higher order terms. Consequently, when $\delta_H = 0$, eqns (6) and (7) reduce to their first order transverse shear deformation (FSDT) counterpart. Furthermore, upon considering $\psi_\alpha \to -(v_{3,\alpha} + b^\rho_\alpha v_\rho)$, the strain measures, eqns (7), reduce to the ones associated with the classical shell theory (CLT).

In the light of the results associated with the SST, in the previous (and forthcoming) equations the covariant differentiation can be performed with respect to the metric at P. In this case, since the Riemann–Christoffel tensor is identically zero, the covariant differentiation is interchangable. In the previously displayed equations partial differentiation is denoted by a comma, $(\,)_{,i} \equiv \partial(\,)/\partial x_i$ while $(\,)|_i$ and $(\,)\|_i$ stand for the covariant differentiation with respect to the space and surface metrics, respectively.

5. EQUATIONS OF MOTION

The geometrical eqns (6) and (7) contain five unknown displacement quantities, namely $v_\alpha(x^\omega, t)$, $v_3(x^\omega, t)$ and $\psi_\alpha(x^\omega, t)$. In order to obtain the governing equations in terms of these unknown functions, five 2-D equations of motion are needed.

They are obtained by taking various moments of the equations of motion of the 3-D non-linear elasticity theory

$$[s^{jr}(\delta^i_r + V^i{}_{,r} + \overset{0}{V}{}^i{}_{,r})]_{,j} = \rho \ddot{V}^i. \tag{8}$$

Employment in eqn (8) of the approximation proper to the SST (implying also the discard of tangential and rotatory inertia terms), followed by consideration of moments of order zero and one of the resulting equations associated with $i = 1, 2$ and of the moment of order zero of the same equations for $i = 3$, results in the 2-D equations of motion:

$$L^{\alpha\beta}|_\beta = 0, \quad M^{\alpha\beta}|_\beta - Q^{\alpha 3} = 0,$$

$$L^{\alpha\beta}(v_{3,\beta} + \overset{0}{v}_{3,\beta})|_\alpha + b_{\mu\alpha}L^{\alpha\mu} + Q^{\alpha 3}|_\alpha + p_3 - m_0\ddot{v}_3 = 0. \tag{9a–c}$$

In these equations p_3 denotes the transversal load, $L^{\alpha\beta}$, $M^{\alpha\beta}$ and $Q^{\alpha 3}$ denote the membrane, stress couples and transverse shear stress resultants, respectively, while m_0 denotes the reduced mass.

6. NONLINEAR BOUNDARY-VALUE PROBLEM

For the problem to be studied in the present work, a most convenient representation of the governing equations is that representing the refined counterpart of the classical von Kármán–Mushtari–Marguerre large deflection shell theory.

To the end of obtaining the governing system in such a form, the procedure developed in a number of previous papers (e.g., Librescu and Chang, 1992, 1993) will be followed. In this spirit, use is made of the Airy stress function $F(x^\alpha, t)$, resulting in the identical fulfilment of eqn (9a). Hence, the compatibility equation for the membrane strains is included as a primary field equation of the nonlinear boundary-value problem. It reads:

$$e^{\alpha\pi}e^{\beta\nu}(\varepsilon_{\alpha\beta|\pi\nu} + \tfrac{1}{2}v_{3|\alpha\beta}v_{3|\nu\pi} + \tfrac{1}{2}\overset{0}{v}_{3|\pi\nu}v_{3|\alpha\beta} + \tfrac{1}{2}v_{3,\pi\nu}\overset{0}{v}_{3,\alpha\beta} + b_{\alpha\beta}v_{3,\pi\nu}) = 0. \tag{10}$$

This equation together with the remaining shell out-of-plane force equilibrium equation and the two moment equilibrium equations, eqns (9c) and (9b), respectively, are basic in the establishment of the governing equations.

Further, as a first step, the inverted form of the pertinent constitutive equation

$$L^{\alpha\beta} = ba^{\alpha\rho}a^{\beta\sigma}\varepsilon_{\sigma\rho} + ca^{\alpha\beta}\varepsilon^\omega_\omega + \frac{4}{h^2}\delta_A da^{\alpha\beta}(v_3|^\rho v_3|_\rho + 2\overset{0}{v}_3|^\rho v_3|_\rho) + \Lambda a^{\alpha\beta}\overset{0}{T}, \tag{11}$$

is needed, which results in

$$\varepsilon_{\alpha\beta} = \tilde{b}a_{\alpha\omega}a_{\beta\rho}L^{\omega\rho} + \tilde{c}a_{\alpha\beta}L^\omega_\omega + \delta_A\tilde{d}(v_3|^\rho v_3|_\rho + 2\overset{0}{v}_3|_\rho v_3|^\rho)a_{\alpha\beta} + \tilde{\Lambda}a_{\alpha\beta}\overset{0}{T}. \tag{12}$$

The expressions of the coefficients b, c, d, Λ and of their tilded counterparts can be found in Librescu and Stein (1991), Librescu and Souza (1991b), and Librescu and Chang (1993a).

Furthermore, the bending stress couples and transverse shear stress resultants are expressed in terms of the rotations ψ_α and the transverse displacement v_3. Substitution of these special constitutive equations into the three remaining shell equations of motions, eqns (9b, c), and into the compatibility equation, eqn (10), results in four coupled partial differential equations in terms of the stress function F, the transverse displacement v_3, and the two rotations ψ_α. By expressing further ψ_α in terms of a potential function $\Gamma(x_\omega, t)$ and of the transverse displacement v_3 (Librescu and Stein, 1991, Librescu and Chang, 1992) the governing equation system can be cast in the form:

$$D\Delta\Delta v_3 - c^{\alpha\omega}c^{\beta\rho}\left\{b_{\alpha\beta}F_{\omega\rho} + (v_{3|\alpha\beta} + \overset{0}{v}_{3|\alpha\beta})F_{\omega\rho} - \left(\frac{B+C}{S} - \delta_A\frac{M}{S}\right)\Delta(b_{\alpha\beta}F_{|\omega\rho} + F_{|\omega\rho}(v_{3|\alpha\beta} + \overset{0}{v}_{3|\alpha\beta}))\right\}$$

$$-\left[p_3 - \left(\frac{B+C}{S} - \delta_A\frac{M}{S}\right)\Delta p_3\right] + m_0\left[\ddot{v}_3 - \left(\frac{B+C}{S} + \delta_A\left(\frac{R}{m_0} - \frac{M}{S}\right)\right)\Delta\ddot{v}_3\right] - \Pi\Delta\overset{1}{T} = 0,$$

$$(\tilde{b}+\tilde{c})\,\Delta\Delta F + \tfrac{1}{2}(\Delta v_3\Delta v_3|_\rho - v_3|^\rho_\lambda v_3|^\lambda_\rho) + (\Delta\overset{0}{v}_3\Delta v_3 - \overset{0}{v}_3|^\pi_\alpha v_3|^\alpha_\pi) + 2H\Delta v_3 - b^\beta_\lambda v_3|^\lambda_\beta) + 2\delta_A\tilde{d}(\Delta v_3|^\rho v_3|_\rho + v_3|^\rho_\lambda v_3|^\lambda_\rho + \Delta\overset{0}{v}_3|^\rho v_3|_\rho + \Delta v_3|^\rho\overset{0}{v}_3|_\rho + 2\overset{0}{v}_3|^\rho_\pi v_3|^\pi_\rho) + \Lambda\Delta\overset{0}{T} = 0,$$

$$\Gamma - \frac{C}{S}\Delta\Gamma = 0. \tag{13a–c}$$

In the preceding equations $\Delta(\equiv(\cdot)|^{\alpha\beta}_{\alpha\beta})$ denotes the 2-D Laplace operator, $c^{\alpha\beta}$ is the 2-D permutation tensor, H denotes the mean curvature of $\sigma(2H \equiv b_{\alpha\beta}a^{\alpha\beta} = 1/R_1 + 1/R_2$, R_1 and R_2 being the principal radii of curvature). In addition A, B, C, D, Λ, Π and $\tilde{b}$, $\tilde{c}$ denote stiffness quantities while M, S and $\tilde{d}$ denote transverse shear stiffness quantities. Their expressions are displayed in the Appendix. Under this form, the equations include the effects of heterogeneity, transverse shear, transverse normal stress, geometric nonlinearities, initial geometric imperfections, shell-curvature, as well as those of non-uniform temperature and pressure fields.

The linear eqn (13c) (of Helmholtz-type) defines the boundary layer effect. Its solution is characterized by a rapid decay when proceeding from the edges towards the interior of the shell. Although v_3 and F appear totally uncoupled with Γ in the *governing equations*, the boundary-value problem remains coupled through the five boundary conditions at each edge of the shell.

For the case of simply supported boundary conditions considered in the present paper (see also Librescu and Stein, 1991), the potential function Γ can be rendered decoupled in the boundary conditions to result as $\partial\Gamma/\partial n = 0$ at a boundary whose outward normal to the contour is $\mathbf{n} = n\mathbf{e}_n$. Since the governing equation for Γ is homogeneous, the solution of eqn (13c), in conjunction with the associated BC is identically zero, and as such, it can be exactly discarded.

7. POSTBUCKLING OF PANELS WITH TANGENTIAL EDGE CONSTRAINTS

In the present study simply supported boundary conditions with varying degrees of tangential edge restraint are considered. The restraint acts in the direction of the outward normal to the panel edge in the surface tangent to the panel at each point of its edges. For these boundary conditions, the transverse displacement at each edge, the bending stress resultant acting about the axis parallel to each edge, and the rotation about the axis normal to each edge (in the tangent plane) are all zero-valued. The degree of tangential edge restraint considered herein is bounded by the cases in which the motion in direction normal to the unloaded edges in the plane tangent to the surface at the panel edges are either unrestrained or completely restrained. For these two cases, the panel edges are referred to herein as movable and immovable, respectively. All intermediate cases are referred to herein as partially movable edges and include elastically restrained edge constraints.

For a movable edge, zero-valued tangential stress resultants are specified at the edge. In contrast, for an immovable edge, the components of the motion that are normal and parallel to the edge in the plane tangent to the surface at the panel edges are restrained and unrestrained, respectively. For this case, the tangential shear stress resultant on the edge is

specified as zero-valued, and the normal displacement to the unloaded edge in the tangent plane is specified as zero-valued in an average sense. To render this displacement zero-valued in an average sense (see Librescu, 1965, 1975), the normal displacement in the tangent plane is obtained in terms of the transverse displacement and Airy's stress function by using the corresponding strain–displacement relation and constitutive equations and then by integrating the resulting expression over the mid-area of the shell. Setting the resulting equation equal to zero, yields the fictitious stress resultant normal to the edge in the plane tangent to the surface at the edge that makes the corresponding normal displacement zero-valued in an average sense.

The analytical procedure used for panels of rectangular $(l_1 \times l_2)$ projection, with opposite edges that are *partially* movable is similar to that previously described for panels with immovable edges. In particular, the average end-shortenings Δ_1 and Δ_2 between edges $x_1 = 0$ and $x_1 = l_1$ and $x_2 = 0$ and $x_2 = l_2$, respectively, are related to the corresponding average compressive edge loads N_{11} and N_{22} by

$$\Delta_1 c_1 = -N_{11}, \quad \Delta_2 c_2 = -N_{22} \tag{14a,b}$$

in the directions normal to the edges $x_1 = 0, l_1$ and $x_2 = 0, l_2$, respectively. From eqns (14) it is apparent that corresponding to the case of immovable edges $x_1 = 0, l_1$ and $x_2 = 0, l_2$, we have $\Delta_1 = 0$ and $\Delta_2 = 0$, implying $c_1 = \infty$ and $c_2 = \infty$, whereas for freely movable edges, implying $c_1 = 0$ and $c_2 = 0$, it results that $N_{11} = 0$ and $N_{22} = 0$. For most practical situations implying intermediate degrees of tangential edge flexibilities, $0 \leqslant c_1 \leqslant \infty$ and $0 \leqslant c_2 \leqslant \infty$. The expressions of the average end-shortening displacements as given by Librescu (1965, 1975) are

$$l_1 l_2 \Delta_1 = -\int_0^{l_1} \int_0^{l_2} \varepsilon_{1,1} \, \mathrm{d}x_2 \, \mathrm{d}x_1,$$

$$l_1 l_2 \Delta_2 = -\int_0^{l_1} \int_0^{l_2} \varepsilon_{2,2} \, \mathrm{d}x_2 \, \mathrm{d}x_1 \tag{15a,b}$$

where ε_1 and ε_2 are the displacements parallel to the x_1 and x_2 directions, respectively. The average compressive edge loads (considered positive in compression) are given by

$$-N_{11} = \frac{1}{l_2} \int_0^{l_2} F_{,22}|_{x_1 = 0, l_1} \, \mathrm{d}x_2,$$

$$-N_{22} = \frac{1}{l_1} \int_0^{l_1} F_{,11}|_{x_2 = 0, l_2} \, \mathrm{d}x_1, \tag{16a,b}$$

where the Airy's function F is represented as

$$F(x_1, x_2, t) = F_1(x_1, x_2, t) - \tfrac{1}{2}[(x_2)^2 N_{11} + (x_1)^2 N_{22}], \tag{17}$$

$F_1(x_\alpha, t)$ being a particular solution of eqn (13b).

Equations (15) are used in conjunction with eqns (14), (7a) to obtain the fictitious edges loads N_{11} and N_{22} that yield the desired normal edge constraint. In order to capture in a more convenient way the whole range of edge constraints, following the procedure presented in Librescu, 1965, the stiffness quantities c_1 and c_2 are redefined in terms of λ_1 and λ_2 as (Librescu *et al.*, 1994b, 1995)

$$\lambda_1 = \frac{(\tilde{b}+\tilde{c})c_1}{1+(\tilde{b}+\tilde{c})c_1}, \quad \lambda_2 = \frac{(\tilde{b}+\tilde{c})c_2}{1+(\tilde{b}+\tilde{c})c_2}, \tag{18a,b}$$

where λ_1 and λ_2 are the newly defined tangential stiffness edge parameters while $(\tilde{b}+\tilde{c})$ is the panel tangential stiffness quantity defined in Librescu and Stein (1991). From eqns (18) it is apparent that $\lambda_1 = 0$ and $\lambda_1 = 1$ correspond to movable and immovable edges at $x_1 = 0$ and l_1, respectively, while $\lambda_2 = 0$ and $\lambda_2 = 1$ correspond to movable and immovable edges at $x_2 = 0$ and l_2, respectively. Partially restrained edges at $x_1 = 0$ and l_1 and $x_2 = 0$ and l_2 implies $0 < \lambda_1 < 1$ and $0 < \lambda_2 < 1$, respectively.

8. SOLUTION OF THE NONLINEAR EQUATIONS

The nonlinear boundary-value problem in the present study is solved using Galerkin's method. Considering the representation

$$\begin{Bmatrix} w_3(x_1, x_2, t) \\ \overset{0}{w}_3(x_1, x_2) \end{Bmatrix} = \begin{Bmatrix} w_{mn}(t) \\ \overset{0}{w}_{mn} \end{Bmatrix} \sin \lambda_m x_1 \sin \mu_n x_2, \tag{19a,b}$$

(where, in order to obtain a most conservative postbuckling prediction (see Seide, 1974), the shape of geometric imperfection is similar to the one of the buckling mode) the out-of-plane boundary conditions are identically fulfilled.

Herein $\lambda_m = m\pi/l_1$, $\mu_n = n\pi/l_2$ while w_{mn} and $\overset{0}{w}_{mn}$ are the modal amplitudes. Similarly, the applied temperature and pressure fields are most generally represented by Navier-type double Fourier sine series. In the present study, the temperature and pressure fields are approximated by

$$\begin{Bmatrix} \overset{0}{T}(x_1, x_2) \\ \overset{1}{T}(x_1, x_2) \\ p_3(x_1, x_2) \end{Bmatrix} = \begin{Bmatrix} \overset{0}{T}_{mn} \\ \overset{1}{T}_{mn} \\ p_{mn} \end{Bmatrix} \sin \lambda_m x_1 \sin \mu_n x_2, \tag{20a–c}$$

The displacement representations (eqns 19) and expression of $\varepsilon_{2\beta}$ (eqn (6a)) are substituted into the compatibility equation, eqn (13b), and the Airy's stress function is obtained by solving the resulting linear non-homogeneous partial differential equation. The remaining nonlinear partial differential equation, eqn (13a), is converted into a set of nonlinear ordinary differential equations using Galerkin's method. This procedure yields an intricate set of $M \times N$ nonlinear ordinary differential equations expressed in symbolic form as

$$A_{rs}\ddot{w}_{rs} + R_{rs}w_{rs} + p_{rs}B_{rs} - \Pi \overset{1}{T}_{rs}C_{rs} + P_1[w_{rs}, \overset{0}{w}_{rs}, \tilde{L}_{11}, \tilde{L}_{22}] + P_2[w_{rs}^2, \overset{0}{w}_{rs}] + P_3[w_{rs}^3, \overset{0}{w}_{rs}] + P_4[w_{rs}, \overset{0}{w}_{rs}, \overset{0}{T}_{rs}, \overset{1}{T}_{rs}] = 0, \quad \sum_{r,s} \tag{21}$$

where the symbol $\sum_{r,s}$ indicates that there is no summation over r and s, and where $r = 1, 2, \ldots, M$ and $s = 1, 2, \ldots, N$. In eqn (21), P_1 and P_4, P_2, and P_3 are linear, quadratic, and cubic polynomials of the unknown modal amplitudes w_{rs}, respectively. The coefficients B_{rs}, C_{rs}, and R_{rs} are constants that depend on the material and geometric properties of the shell and $\tilde{L}_{11}(\equiv N_{11}l_1^2/(\pi^4 D))$ and $\tilde{L}_{22}(\equiv N_{22}l_1^2/(\pi^4 D))$ represent the dimensionless normalized tangential edge loads normal to the edges $x_1 = 0, l_2$ and $x_2 = 0, l_2$, respectively.

9. EQUATIONS FOR STATIC EQUILIBRIUM STATES AND SMALL VIBRATIONS

The main emphasis of the present study is the static postbuckling and vibrational behavior of flat and curved panels that are loaded quasistatically into the pre/postbuckling range. To obtain equations governing the static pre postbuckling equilibrium states and

small vibrations about these equilibrium states, the unknown modal amplitudes are expressed as

$$w_{rs}(t) = \bar{w}_{rs} + \bar{\bar{w}}_{rs}(t), \tag{22}$$

where $\bar{\bar{w}}_{rs}(t)$ represents small vibrations about a mean static equilibrium configuration described by $\bar{w}_{rs}$. The disturbances $\bar{\bar{w}}_{rs}$ are considered small compared to both $\bar{w}_{rs}$ and the imperfection amplitude $\overset{0}{w}_{rs}$ in the sense of

$$[\bar{\bar{w}}_{rs}(t)]^2 \ll \bar{w}_{rs}, \overset{0}{w}_{rs}, \tag{23}$$

for all values of the indices r and s. The equations for the static prebuckling and postbuckling equilibrium states are obtained by discarding the inertia terms given by $A_{rs}\ddot{w}_{rs}$ in eqn (21). The solution to the resulting equation is $\bar{w}_{rs}$. The equations for small vibrations about a given static equilibrium state are then obtained by substituting eqn (22) into eqn (21) and enforcing the smallness condition given by eqn (23). The resulting equations of motion are given by

$$A_{rs}\ddot{\bar{\bar{w}}}_{rs}(t) + G_{rs}\bar{\bar{w}}_{rs}(t) = 0, \quad \sum_{rs}, \tag{24}$$

where

$$G_{rs} = G_{rs}(\bar{w}_{rs}, \bar{w}_{rs}^2, \bar{w}_{rs}^3, \overset{0}{w}_{rs}, p_{rs}, \overset{0}{T}_{rs}, \overset{1}{T}_{rs}) \tag{25}$$

for values of $r = 1, 2, \ldots, M$ and $s = 1, 2, \ldots, N$. The constant coefficients A_{rs} are functions of the material and geometric properties of the panel.

Equation (24) governs small vibrations about a given equilibrium state and are solved for harmonic motion by expressing $\bar{\bar{w}}_{rs}(t)$ as

$$\bar{\bar{w}}_{rs}(t) = \tilde{w}_{rs} \exp(i\omega_{rs}t). \tag{26}$$

Substitution of eqn (26) into eqn (24) yields an algebraic eigenvalue problem given by

$$G_{rs}\tilde{w}_{rs} = \omega_{rs}^2 A_{rs}\tilde{w}_{rs}, \quad \sum_{rs}. \tag{27}$$

for values of $r = 1, 2, \ldots, M$ and $s = 1, 2, \ldots, N$. The frequencies ω_{rs} in eqn (27) are the unknown quantities to be found and the corresponding amplitudes $\tilde{w}_{rs}$ are indeterminate.

10. COMPUTATIONAL ASPECTS

In the present study, two distinct types of thermal loadings are considered. One of them corresponds to a uniform through thickness temperature distribution $\overset{0}{T} = \overset{0}{T}(x_\alpha)$, while the second one is associated with a linear through-the-thickness temperature variation $\overset{0}{T}(x_\alpha) + x_3\overset{1}{T}(x_\alpha)$. These two types of thermal loadings will be referred to as TL1 and TL2, respectively. In addition, in some instances explicitly mentioned, the panel is assumed to be acted on also by edge and/or lateral pre-loads.

The static equilibrium configuration for a given flat or curved panel is obtained by solving the static counterpart of the nonlinear algebraic equation system, eqns (21), via Newton's method. After obtaining the static equilibrium configuration of the panel for given values of the loading parameters, the coefficients A_{rs} and G_{rs} in eqns (27) are computed and the linear algebraic eigenvalue problem is solved. In some instances, eqns (27) possess negative eigenvalues that correspond to pure imaginary fundamental vibration frequencies.

For the panels investigated herein, the pure imaginary fundamental frequencies correspond to unstable branches of postbuckling equilibrium path.

11. NUMERICAL ILLUSTRATIONS

The results presented in the present paper are for small vibrations about the static prebuckling and postbuckling equilibrium states of simply supported flat and curved panels. The panels considered have a square planform with dimensions $l_1 = l_2 = l$ and consist of either a single or three layers of elastic transversely isotropic material. In all numerical results presented herein, the following input data characterizing the thermoelastic material properties have been used:

$$\nu' = 0.2, \quad \lambda/E = -1.15 \times 10^{-5} \text{ in/in/}^\circ\text{F}, \quad \lambda/\lambda' = 1.4286, \quad \text{and} \quad E/E' = 5.$$

For the three-layer panels one assumes that the core-layer is twice as thick as each of the face-layers. In addition, throughout these results it was assumed that the elastic moduli and thermal compliance coefficients are defined in terms of non-dimensional ratios as:

for the face-layers

$$(E/E')_f = 5; \quad (E/G')_f = 10, \quad (\lambda/\lambda')_f = 1.4286, \quad (\lambda/E)_f = -1.15 \times 10^{-5} \text{ in/in/}^\circ\text{F}$$

and for the core-layer

$$(E/E')_c = 2; \quad (E/G')_c = 30, \quad (\lambda/\lambda')_c = 1.21413, \quad (\lambda/E)_c = -4.8875 \times 10^{-5} \text{ in/in/}^\circ\text{F}.$$

It was also postulated that $E_f/E_c = 10$.

In these expressions the indices f and c identify the affiliation of the respective quantities to the face and core layer, respectively. The considered numerical data imply that the core layer is more shear-deformable than the face layers, a behavior which is commonly considered in sandwich type constructions.

In all the obtained results, unless stated otherwise, it was considered $\delta_H = 1$, implying that the higher order effects have been incorporated. In addition, it was considered invariably $\delta_A = 1$, thus avoiding the contradiction implied by the simultaneous consideration of $s^{33} = 0$ and $e_{33} = 0$. It should also be mentioned that in the displayed results T_c, T_i, p, $\delta(\equiv w_{11}/h)$, and $\delta_0(\equiv \overset{0}{w}_{11}/h)$ stand for the amplitudes of the respective quantities at the center ($x_1 = l_1/2$, $x_2 = l_2/2$) of the panel.

12. RESULTS FOR FLAT PANELS

The effects of tangential edge restraints on small vibrations about the static prebuckling and postbuckling equilibrium state of geometrically perfect simply supported flat three layer panels are presented in Figs 1 and 2. The panel considered in these illustrations features movable edges at $x_1 = 0$ and $x = l_1$ and varying degrees of edge constraint at $x_2 = 0$ and $x_2 = l_2$. In the figures $\bar{\omega}^2(\equiv m_0 l_1^4 \omega^2/(\pi^2 D))$ defines the square of dimensionless fundamental frequency. Whereas Fig. 1 depicts the frequency-temperature interaction for the case of a uniform through thickness temperature rise, Fig. 2 corresponds to the case of panels subjected to a thickness-wise temperature gradient.

In the former case, buckling occurs for those $\overset{0}{T}(\equiv \overset{0}{T}_{11})$ (indicated by the filled circles in the figure) rendering $\bar{\omega}^2 \to 0$. Consistent with the features already discussed in Librescu *et al.* (1994b, 1995), Fig. 1 reveals that with the increase of the degree of restraint of edges $x_2 = 0, l_2$, the buckling temperature decreases. Moreover, Fig. 1 shows also that, in the prebuckling range, the increase of λ_2 results in the decrease of natural frequencies, whereas in the postbuckling range the opposite trend becomes apparent. In the case of the TL2 type loading, since the panels begin deflecting at the onset of the thermal rise, tensile stresses are

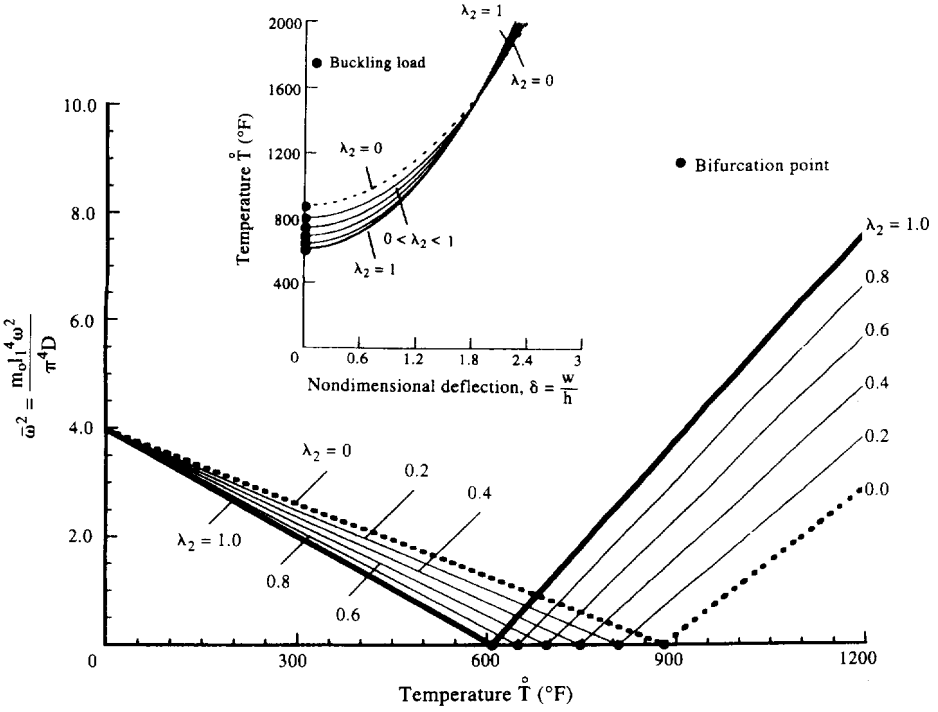

Fig. 1. Effect of in-plane edge constraints on the frequency (squared)–temperature interaction of three-layered flat panels ($l_1/h = 100$, TL1, $\bar{L}_{11} = 0$, $\delta_0 = 0$, $\lambda_1 = 0$). The static counterpart is displayed in the inset.

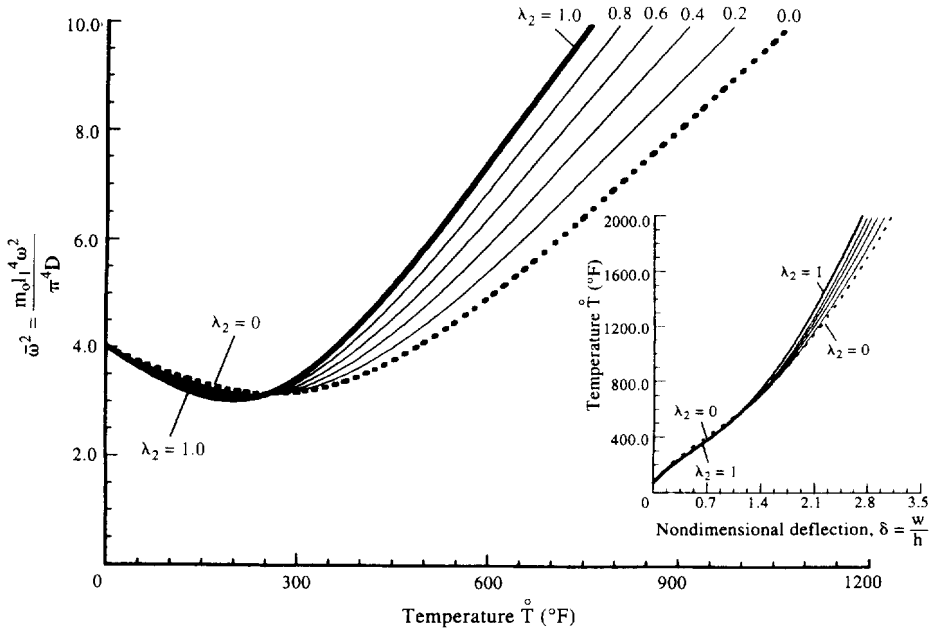

Fig. 2. The counterpart of Fig. 1 for TL2 type loading, $T_c = 70$ F, $\lambda_1 = 0$.

generated resulting in the stiffening of the panel. This explains the steep increase of eigenfrequencies with $\overset{0}{T}$, following a slight decrease of them.

In this case, as Fig. 2 reveals, in contrast to the case corresponding to Fig. 1, in addition to the fact that the eigenfrequencies cannot become zero-valued (implying that the panel does not experience buckling bifurcation), the increase of the fundamental frequencies

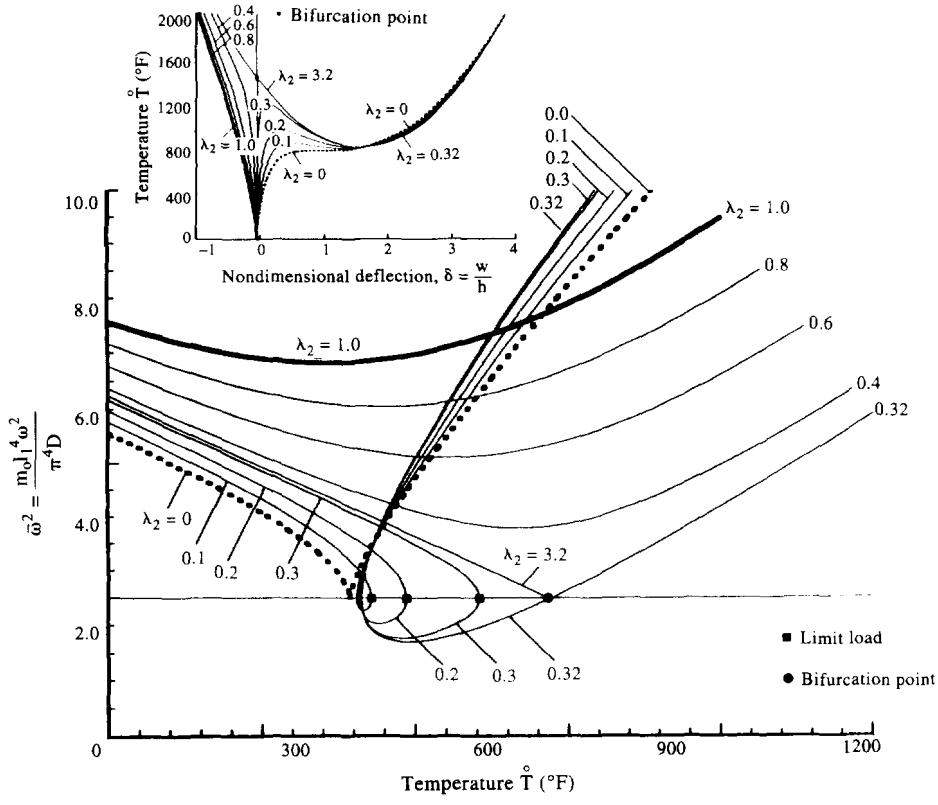

Fig. 3. Effect of tangential constraints of straight edge on the squared frequency–temperature interaction of geometrically perfect circular cylindrical panels ($l_1/h = 100$, $l_1/R_1 = 0$, $l_2/R_2 = 0.1$, TL2 ($T_c = 70$°F), $\tilde{L}_{11} = 0$, $\delta_0 = 0$). The curved edges are movable ($\lambda_1 = 0$). The static postbuckling counterpart is displayed in the inset.

starts at much smaller values of the temperature rise. To facilitate understanding, in both figures their static counterpart is displayed as a small inset.

13. RESULTS FOR CURVED PANELS

The effects of tangential edge restraints on the frequency–temperature interaction are presented, for the case of cylindrical panels, in Figs 3 and 4.

The results in these figures are obtained for geometrically perfect circular cylindrical panels ($l_2/R_2 = 0.1$) subjected to the TL2 type loadings. Their straight edges are considered to feature various degrees of tangential constraints, implying that at these edges $0 \leqslant \lambda_2 \leqslant 1$, whereas the curved edges feature (see Figs 3 and 4) movable ($\lambda_1 = 0$) and immovable ($\lambda_1 = 1$) edge constraints, respectively.

The results emerging from these graphs reveal that corresponding to $\lambda_1 = 0$ and 1, for $\lambda_2 = 0.32$ and $\lambda_2 = 0.37$ the respective panels exhibit buckling bifurcation while for $\lambda_2 < 0.32$ and $\lambda_2 < 0.37$, limit temperature loads are experienced, respectively.

The response curves indicate that for degrees of the tangential constraints of straight edges lower or equal with the ones resulting in the buckling bifurcation, the fundamental frequency decreases monotonically with increasing $\overset{0}{T}$ in the prebuckling/prelimit ranges, whereas for larger degrees of the edge constraint, a monotonous increase in the fundamental frequency is experienced.

At buckling/collapse points the further increase of $\overset{0}{T}$ results in a jump on the stable path corresponding to real values of fundamental frequency. The insets in the Figs 3 and 4 depicting the static postbuckling counterparts aim to provide a more comprehensive understanding of the effects played by the tangential edge constraints.

Figure 5 represents the counterpart of Fig. 3 obtained for the case of the uniform temperature distribution through the wall thickness (i.e., of the TL1 type loading). The

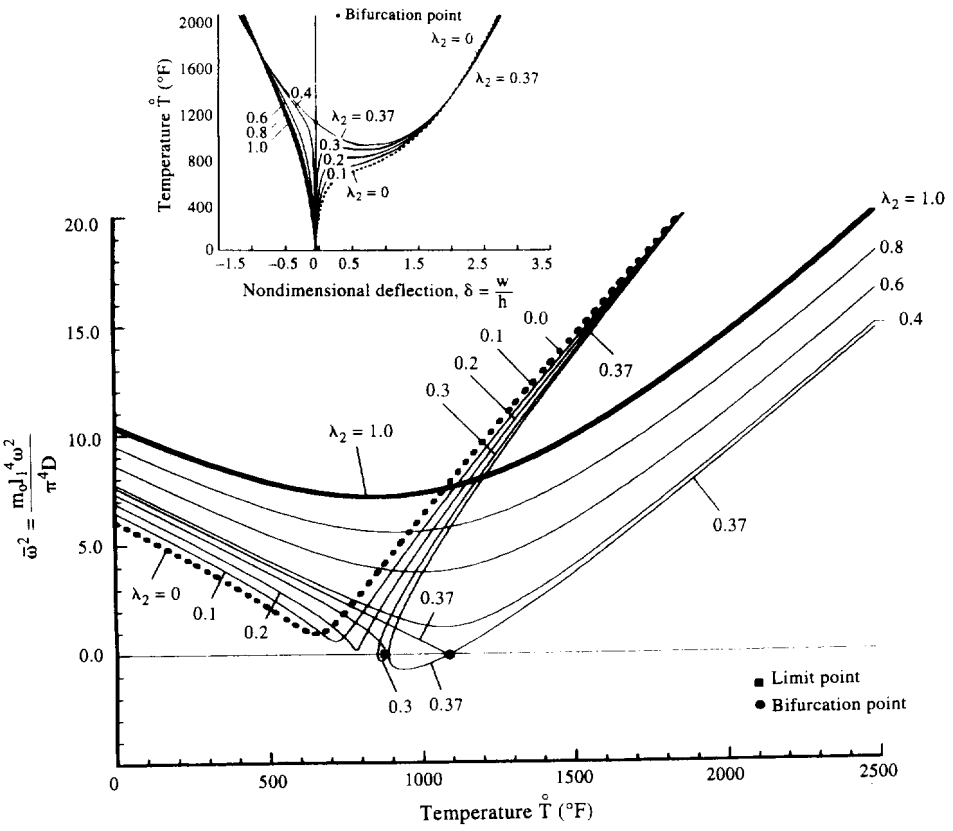

Fig. 4. The counterpart of the case depicted in Fig. 3 corresponding to ($\lambda_1 = 1$). The static post-buckling counterpart is displayed in the inset.

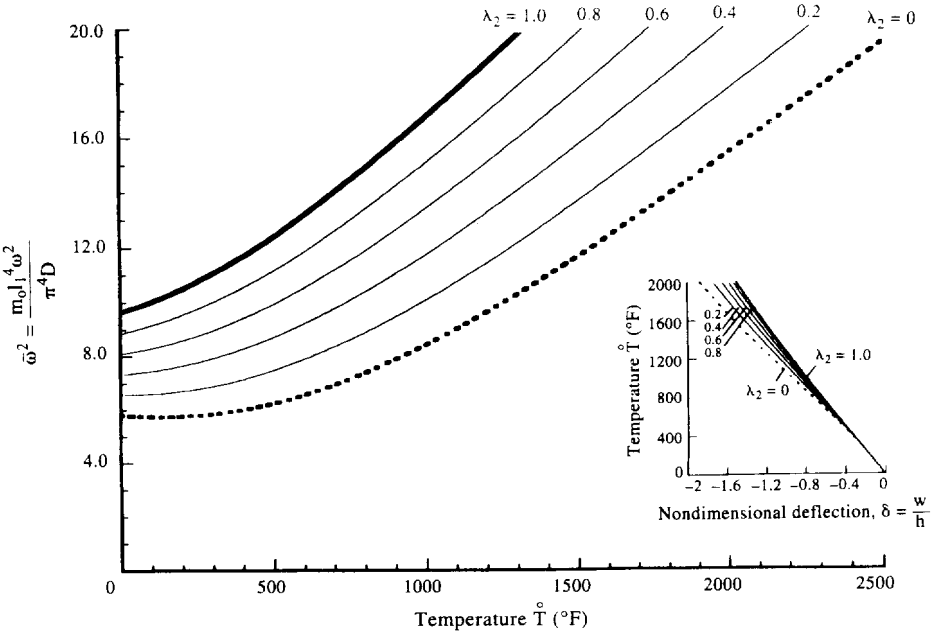

Fig. 5. The counterpart of the case considered in Fig. 3 for the TL1 type loading.

results associated with this case reveal that with the temperature rise, a continuous increase of natural frequencies is obtained. They also show that the increase of the degree of restraint of straight edges yields a significant increase of natural frequencies. The static counterpart of this case, appearing as an inset, adds to the understanding of the response behavior.

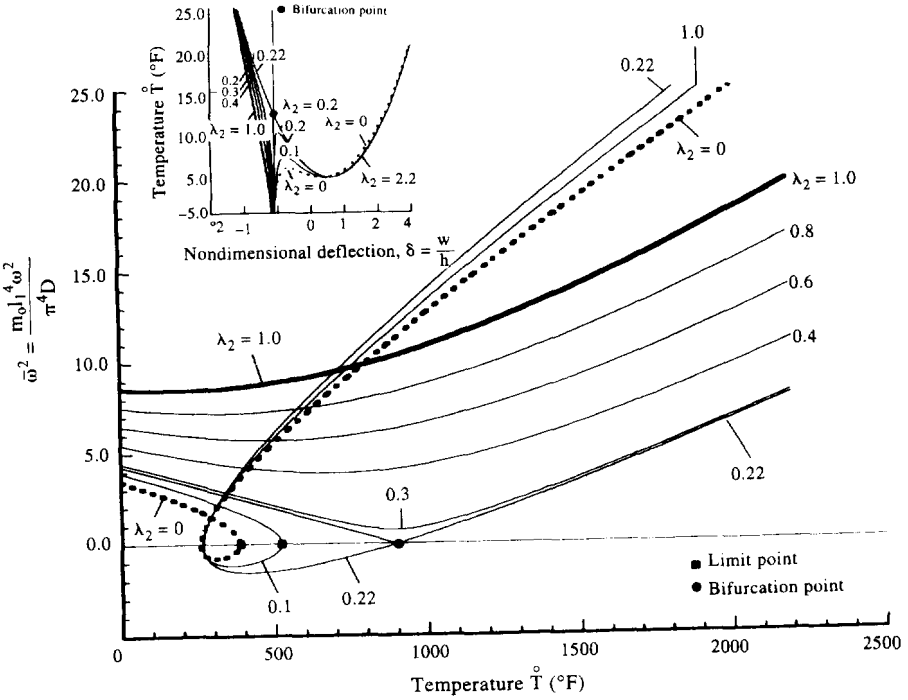

Fig. 6. The counterpart of the case depicted in Fig. 3 for $\tilde{L}_{11} = 2.5$.

The effect of an uniaxially sub-critical compressive edge preload held fixed is presented in Fig. 6. Compared to its counterpart associated with $\tilde{L}_{11} = 0$ (Fig. 3), it becomes apparent that it contributes to the decrease of both the thermal buckling load and natural frequencies. However, in the post-buckling/prelimit regimes the increase of natural frequencies is stronger than in the case of the unloaded edge counterpart. Moreover, in contrast to the case of the unloaded edges (Fig. 3), in the present one, the cylindrical panel featuring movable straight edges experiences snap-through buckling.

The effect of initial geometric imperfection is illustrated in Fig. 7. As compared to the geometrically perfect panel counterpart, Fig. 3, in this case, the results reveal that larger degrees of tangential edge restraint are needed to yield the thermal buckling bifurcation. This implies that in this case there is a more limited interval of degrees of edge constraints for which the imperfection–sensitivity behavior featured by the curved panel can be changed in an imperfection–insensitivity one.

In Fig. 8, the case of a very shallow and geometrically imperfect circular cylindrical panel compressed by the sub-critical pre-load $\tilde{L}_{22}$ is considered. It is assumed that the panel features movable straight edges and various degrees of restraint of the curved edges. In this case it is seen that the panel does not experience buckling bifurcation and that with the increase of tangential constraints of curved edges, a delay of the occurrence of the snap-through, in the sense of Birman and Bert, 1993, is occurring. This delayed snap-through buckling has, however, to be payed by the increase of the intensity of the snap-through, a trend which is valid in both the dynamic and static situations (see the inset). Moreover, the results reveal that in contrast to the trend in Figs 3–7, in this case there is no benign postbuckling behavior in the sense of a monotonous increase of the deflection/frequencies with the rise of the temperature. Based on the results obtained recently (see the paper by Librescu *et al.*, 1994), a similar trend can be obtained; for example, when associated with the configuration in Fig. 7, larger initial geometric imperfections are involved.

In Fig. 9 the effect of the degree of restraint of straight edges on the frequency–temperature interaction of geometrically perfect circular cylindrical panel is highlighted. The panel is subjected to the pre-loads consisting of the uniaxial pre-critical compression $\tilde{L}_{11}$ and a lateral pressure of amplitude $p(\equiv p_0 l_1^4/(Dh)$ where $p_0 \equiv p_{11})$. Herein the curved edges are considered perfectly movable.

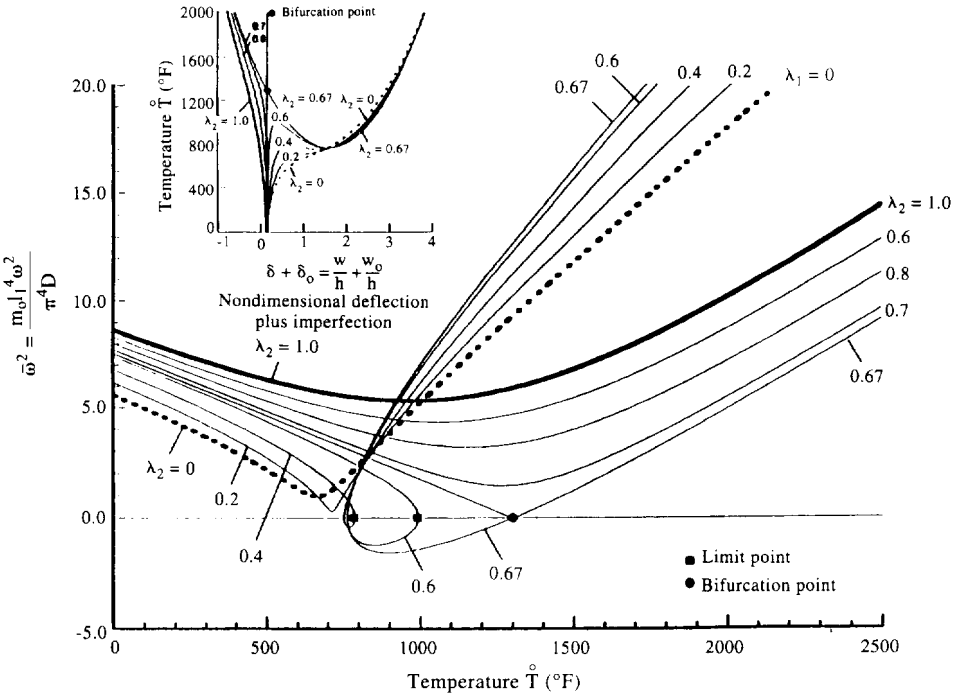

Fig. 7. The counterpart of the case depicted in Fig. 3 for $\delta_0 = 0.2$.

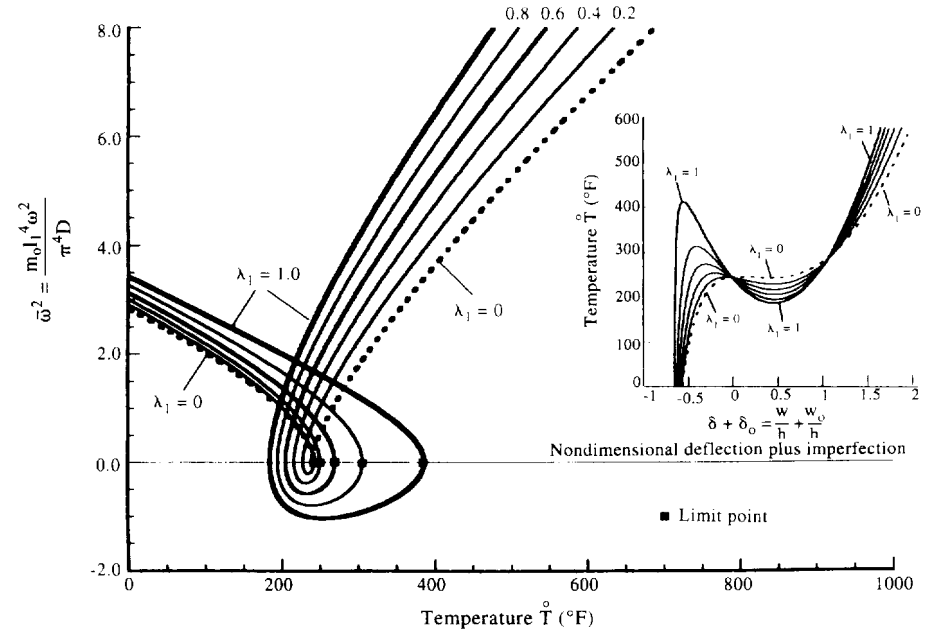

Fig. 8. Effect of tangential constraints of curved edges on the frequency temperature interaction of a very shallow and geometrically imperfect circular cylindrical three-layer panel ($l_1/h = 100$, $l_1/R_1 = 0$; $l_2 = 0.03$; $\delta_0 = 0.2$, $\tilde{L}_{22} = 0.75$, TL2 ($T_i = 70$ F)). The straight edges are assumed to be movable ($\lambda_2 = 0$).

Similarly to the previously investigated cases, also for a laterally loaded panel, consistent with its overall geometric and mechanical characteristics, there is a special degree of the tangential constraint of the straight edges yielding the thermal buckling-bifurcation. It may also be seen that the non-linear response featured in this case follows, qualitatively, the trend emerging, e.g., in the case of Fig. 6 above.

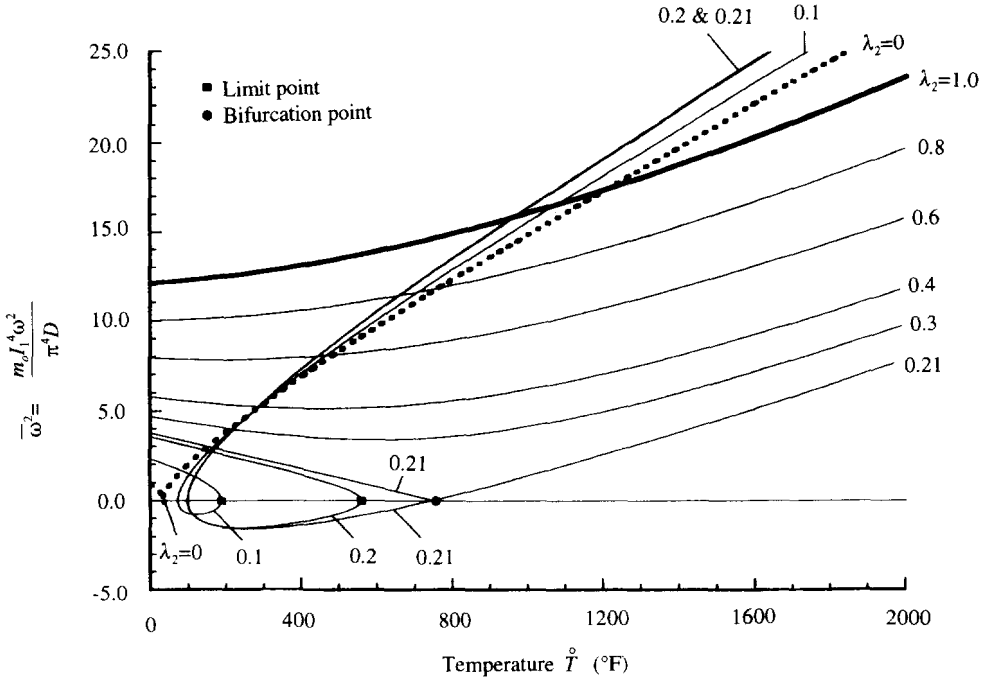

Fig. 9. Effect of tangential constraints of straight edges upon the frequency–temperature interaction of geometrically circular cylindrical panels subjected to combined mechanical pre-loads ($l_1/R_1 = 0$, $l_2/R_2 = 0.15$, TL2 ($T_3 = 70$), $\tilde{L}_{11} = 3$, $p = 2.5$, $\delta_0 = 0$). The curved edges are assumed to be movable ($\lambda_1 = 0$).

Figure 10 displays the frequency–lateral pressure interaction of geometrically perfect spherical caps exposed to the TL2 type loading characterized by the temperature of amplitudes $T_e = 70$ F and $T_i = 1000$ F held fixed. The results reveal that the various combinations of tangential edge constraints can result either in lower eigenfrequencies in the pre/post-limit ranges (but featuring a milder snap-through), or in large eigenfrequencies in both ranges (but featuring a more severe snap-through behavior). It should be noticed in this respect the qualitative similarity of the non-linear response emerging in this case, with that occurring in the conditions pertinent to Fig. 8.

In Fig. 11 the frequency–temperature interaction for the case of a *single-layered* circular cylindrical panel is displayed. It is supposed that the panel is subjected to the axial pre-load $\tilde{L}_{11}(= 50\%\tilde{L}_{cr})$, that the straight edges can be movable or immovable and that the curved edges are invariably movable. The results reveal that the combination of edge constraints ($\lambda_1 = 0, \lambda_2 = 1$) is less beneficial than that implying ($\lambda_1 = 0, \lambda_2 = 0$), in the sense that in the former case a snap-through buckling can appear whereas in the latter one, a monotonous increase of the eigenfrequencies with the temperature rise is experienced. This conclusion remains valid within both the classical ($E/G' = 0$) and shear deformable ($E/G' = 30$) shell models.

The same graph reveals that, as compared to the actual panel featuring transverse shear flexibility, the classical shell theory results in the overestimation of natural frequencies in the pre-limit loading range and in their underestimation in the post-limit one. Moreover, in contrast to the shear deformable shell model, the classical theory inadvertently predicts the impossibility of occurrence of the snap-buckling. Last but not least, the results of this graph reveal that associated with the FSDT, the shear correction $K^2 = 5/6$ provides predictions in closest agreement with those based on HSDT. However, previous results reveal (see Librescu *et al.*, 1993b,c, 1994, 1995) that for a *laminated* panel $K^2 = 2/3$ is a more reliable shear coefficient.

14. CONCLUSIONS AND DISCUSSION

The frequency–temperature interaction and the influence exerted thereof by the tangential edge constraints of flat/curved panels was examined. The effects played by the

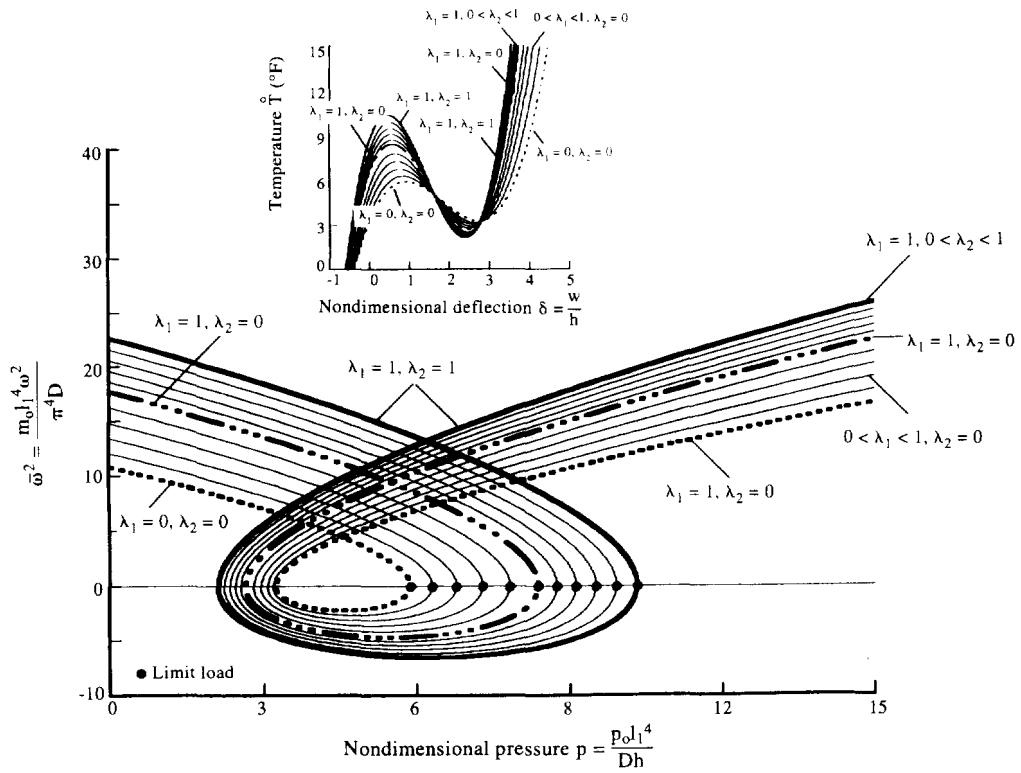

Fig. 10. Effect of tangential edge constraints on the squared frequency lateral load interaction of a geometrically-perfect spherical cap.

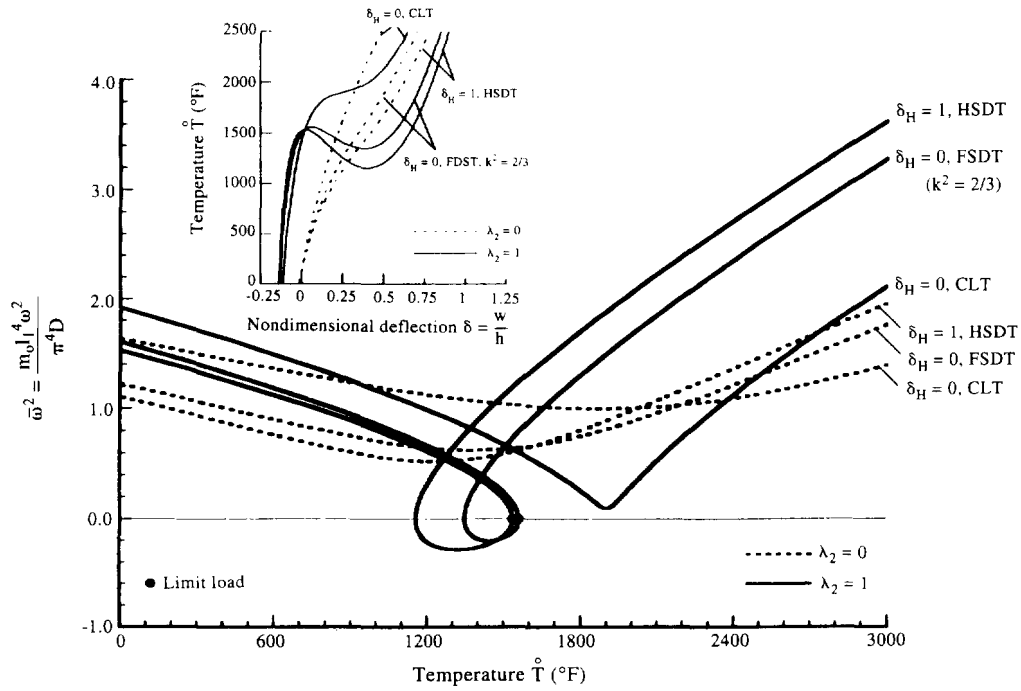

Fig. 11. Effect of tangential constraints of straight edges, of transverse shear flexibility and of higher order terms on the frequency–temperature interaction of geometrically perfect single-layer circular cylindrical panel ($l_1/R_1 = 0$, $l_2/R_2 = 0.1$, $l_1/h = 20$, TL2 ($T_c = 70$ F), $\bar{L}_{11} = 50\%\bar{L}_{cr}$). The curved edges are assumed to be movable ($\lambda_1 = 0$). Predictions based on the FSDT with $K^2 = 5/6$ coincide with those based on the HSDT.

compressive/lateral pre-loads as well as by initial geometric imperfection are also considered. The temperature field $T = T(x_\alpha, x_3)$ used in the analysis is considered either

uniform through the wall thickness (i.e., $T \to T(x_\omega)$) or is assumed to be the result of the superposition of a uniform and a thickness-wise temperature gradient (i.e., $T \to \overset{0}{T}(x_\omega) + x_3 \overset{1}{T}(x_\omega)$). Throughout this paper simply-supported flat and curved panels of a square projection on the plane P are considered. It was shown that the degree of tangential edge restraint can, in general, to significantly enhance the static/dynamic response, and, in particular, to delay the occurrence of the snap-through buckling, remove completely this damaging phenomenon by rendering the postbuckling behavior a benign one and to render, in some cases, a curved panel insensitive to initial geometric imperfections.

It should be noted that the trend revealed in a number of plots (e.g., Figs 3, 4) is similar to the one experienced by a structure featuring *asymmetric buckling bifurcation* in the sense of Budiansky and Hutchinson (1966), Hutchinson and Koiter (1970) and Budiansky (1974).

For the present case, the "perfect" structure considered in these works corresponds to the one featuring a degree of edge constraint (denoted, for convenience, as λ_*) resulting in the buckling bifurcation.

The positive(negative) imperfections resulting in a detrimental (benign) postbuckling behavior, will correspond in this case to the degrees of edge restraints $\lambda < \lambda_*(\lambda > \lambda_*)$. Based on the obtained results one can conclude that the type of asymmetric buckling bifurcation can occur in any curved structure featuring tangential edge constraints.

Moreover, one can design such a structure featuring asymmetric buckling bifurcation and get for $\lambda > \lambda_*$ a benign postbuckling and vibrational behavior. It should be mentioned in passing that such situations are likely to occur also in the case, e.g., of the postbuckling of a non-symmetrically laminated panels (Carerra, 1992, and Vinogradov and Dwyer, 1994). For such a case, the degree of bending-stretching coupling induced by the structural non-symmetry should play a similar role to the degree of tangential edge constraint.

It is hoped that this work will contribute to a better understanding and design of flat and curved panels exposed to complex thermomechanical loads and featuring tangential edge constraints and initial geometric imperfections.

Acknowledgements—The work reported herein was partially supported by NASA Grant NAG-1-1300. The technical discussions with Drs J. H. Starnes, Jr. and M. P. Nemeth of NASA Langley Research Center, Hampton, VA and their suggestions on a number of issues related with this paper are gratefully acknowledged.

REFERENCES

Birman, V. and Bert, C. W. (1993). Buckling and post-buckling of composite plates and shells subjected to elevated temperature. *ASME, Journal of Applied Mechanics* **60,** 514–519.

Budiansky, B. (1974). Theory of buckling and post-buckling behavior of elastic structures. In *Advances in Applied Mechanics* (edited by Chia-Shun Yih), Vol. 14, pp. 1–65, Academic Press, New York.

Budiansky, B. and Hutchinson, J. W. (1996). Asurvey of some buckling problems. *AIAA Journal* **3,** 1505–1510.

Carrera, E. (1992). Some models to study the non-linear response of asymmetrically laminated plates in cylindrical bending. Publication 70/92. Politecnico di Torino, Dept. of Aeronautical/Aerospace Engng.

Garber, A. M. (1963). Pyrolitic materials for thermal protection systems. *Aerospace Engineering*, 126–137.

Green, A. E. and Zerna, W. (1968). *Theoretical Elasticity*, Clarendon Press, Oxford.

Hutchinson, J. W. and Koiter, W. T. (1970). Postbuckling theory. *Applied Mechanics Review* **23,** 1353–1366.

Librescu, L. (1965). Aeroelastic stability of orthotropic heterogeneous thin panels in the vicinity of the flutter critical boundary. Part one: simply supported panels. *Journal de Mécanique* **4,** 51–76.

Librescu, L. (1975). *Elasto-Statics and Kinetics of Anisotropic and Heterogeneous Shell-Type Structures*, Noordhoff International, Leyden, The Netherlands.

Librescu, L. and Stein, M. (1991a). A geometrically nonlinear theory of transversely-isotropic laminated composite plates and its use in the postbuckling analysis. *Thin Walled Structures* **11,** 177–201.

Librescu, L. and Souza, M. A. (1991b). Thermal postbuckling behavior of geometrically imperfect shear-deformable composite panels. In *Mechanics of Composites at Elevated and Cryogenic Temperatures* (eds. S. N. Singhal, W. F. Jones and C. T. Herakovich), pp. 305–321, ASME, New York.

Librescu, L. and Chang, M.-Y. (1992). Post-buckling and imperfection sensitivity of shear deformable composite doubly-curved panels. *International Journal of Solids and Structures* **29,** 1065–1983.

Librescu, L. and Chang, M. Y. (1993a). Effects of geometric imperfections on vibration of compressed shear deformable laminated composite curved panels. *Acta Mechanica* **96,** 203–224.

Librescu, L., Lin, W., Nemeth, M. P. and Starnes, Jr., J. H. (1993b). Vibration of geometrically imperfect laminated flat and shallow curved panels subjected to heating and a system of mechanical loadings. Presented at the Tenth DoD/NASA/FAA Conference on Fibrous Composites in Structural Design, Hilton Head Island, SC, 1–4 November (appeared in *Journal of Spacecraft and Rockets* **33,** 285–291 (1996)).

Librescu, L., Lin, W., Nemeth, M. P. and Starnes, Jr., J. H. (1993c). Classical versus non-classical postbuckling behavior of laminated composite panels under complex loading conditions. In *Non-Classical Problems of the Theory and Behavior of Structures Exposed to Complex Environmental Conditions* (ed. L. Librescu), ASME, NY, pp. 169–182.

Librescu, L., Lin, W., Nemeth, M. P. and Starnes, Jr., J. H., (1994a). Effects of a thermal field on frequency-load interaction of geometrically imperfect shallow curved panels. *Paper AIAA*-94-1342, *AIAA/ASME/ASCE/AHS/ASC 35th Structures, Structural Dynamics and Materials Conference*, 18–20 April (appeared in *AIAA Journal* **34,** 166–177 (1996)).

Librescu, L., Lin, W., Nemeth, M. P. and Starnes, Jr., J. H. (1994b). Effects of tangential edge constraints on the postbuckling behavior of flat and curved panels subjected to thermal and mechanical loads. In *Buckling and Postbuckling of Composite Structures* (ed. A. K. Noor), ASME, NY, pp. 55–71.

Librescu, L., Lin, W., Nemeth, M. P. and Starnes, Jr., J. H. (1995). Thermomechanical postbuckling of geometrically imperfect flat and curved panels taking into account tangential edge constraints. *Journal of Thermal Stresses* **18,** 465–482.

Naghdi, P. M. (1963). Foundations of elastic shell theory. *Progress of Solid Mechanics* **4,** 1–86.

Reddy, J. N. and Liu, C. F. (1987). A higher-order theory for geometrically nonlinear analysis of composite laminates. *NASA Contract Report* 4056.

Seide, P. (1974). A reexamination of Koiter's theory of initial postbuckling behavior and imperfection sensitivity of structures. In *Thin Shell Structures: Theory, Experiment and Design* (edited by C. Y. Fung and E. E. Sechler), pp. 59–80, Prentice-Hall, New Jersey.

Vinogradov, A. M. and Dwyer, J. F. (1994). Nonlinear stability analysis of multi-layered asymmetric laminates. Presented at *Twelfth U.S. National Congress of Applied Mechanics*, University of Washington, Seattle, WA, 27 June–1 July.

Woods, P. H. (1976). Pyrolitic graphite for high pressure, high temperature applications. *AIAA Paper* 76-605, 2805–2823.

APPENDIX

The stiffness quantities associated with a transversely-isotropic symmetrically laminated composite panel appearing in eqns (13a–c).

$$A = \delta_H \frac{8}{15h^2}\left[\bar{E}_{(m+1)}\, h^5_{(m+1)} + \sum_{r=1}^{m} \bar{E}_{(r)}(h^5_{r} - h^5_{r+1})\right],$$

$$B = \frac{1}{3}\left[E_{m+1}\,(1+\nu_{(m+1)})h^3_{(m+1)} + \sum_{r=1}^{m} \bar{E}_{r}(1+\nu_{(r)})(h^3_{(r)} - h^3_{r+1})\right]$$

$$-\delta_H \frac{4}{15h^2}\left[\bar{E}_{(m+1)}(1+\nu_{(m+1)})h^5_{m+1} + \sum_{r=1}^{m} \bar{E}_{(r)}(1+\nu_{(r)})(h^5_{(r)} - h^5_{(r+1)})\right],$$

$$C = \frac{1}{3}\left[\bar{E}_{m+1}\,(1-\nu_{(m+1)})h^3_{(m+1)} + \sum_{r=1}^{m} \bar{E}_{r}(1-\nu_{(r)})(h^3_{r} - h^3_{(r+1)})\right]$$

$$-\delta_H \frac{4}{15h^2}\left[\bar{E}_{(m+1)}(1-\nu_{(m+1)})h^5_{m+1} + \sum_{r=1}^{m} \bar{E}_{(r)}(1-\nu_{(r)})(h^5_{(r)} - h^5_{(r+1)})\right],$$

$$S = 2G'_{(m+1)}h_{(m+1)} + 2\sum_{r=1}^{m} G'_{(r)}(h_{r} - h_{r+1})$$

$$-\delta_H \frac{8}{3h^2}\left[G'_{(m+1)}h^3_{(m+1)} + \sum_{r=1}^{m} G'_{r}(h^3_{(r)} - h^3_{(r+1)})\right],$$

$$M = \frac{2}{3}\left\{\left[\frac{\nu'_{(m+1)}E_{(m+1)}G'_{(m+1)}}{E'_{(m+1)}(1-\nu_{(m+1)})}h^3_{(m+1)} + \sum_{r=1}^{m}\frac{\nu'_{r}E_{(r)}G'_{(r)}}{E'_{r}(1-\nu_{(r)})}(h^3_{(r)} - h^3_{(r+1)})\right.\right.$$

$$\left.\left.-\delta_H \frac{4}{5h^2}\left[\frac{\nu'_{(m+1)}E_{(m+1)}G'_{(m+1)}}{E'_{(m+1)}(1-\nu_{(m+1)})}h^5_{m+1} + \sum_{r=1}^{m}\frac{\nu'_{(r)}E_{(r)}G'_{(r)}}{E'_{(r)}(1-\nu_{(r)})}(h^5_{(r)} - h^5_{(r+1)})\right]\right\}$$

$$R = \frac{2}{3}\left[\rho_{(m+1)}\frac{E_{(m+1)}\nu'_{(m+1)}}{E'_{(m+1)}(1-\nu_{(m+1)})}h^3_{(m+1)}\right.$$

$$\left.+\sum_{r=1}^{m}\rho_{(r)}\frac{E_{r}\nu'_{r}}{E'_{r}(1-\nu_{r})}(h^3_{(r)} - h^3_{r+1})\right],$$

$$\Lambda = 2\left\{\tilde{\lambda}_{(m+1)}h_{(m+1)} + \sum_{r=1}^{m}\tilde{\lambda}_{(r)}(h_{(r)} - h_{r+1})\right\},$$

$$\Pi = \frac{2}{3}\left\{\tilde{\lambda}_{(m+1)}h^3_{(m+1)} + \sum_{r=1}^{m}\tilde{\lambda}_{(r)}(h^3_{r} - h^3_{r+1})\right\}.$$

$$D(\equiv A+B+C)=\frac{2}{3}\left[\bar{E}_{\langle m+1\rangle}h^3_{\langle m-1\rangle}+\sum_{r=1}^{m}\bar{E}_{\langle r\rangle}(h^3_{\langle r\rangle}-h^3_{\langle r+1\rangle})\right].$$

Here $\bar{E}\equiv E/(1-\nu^2)$.

$$\tilde{b}=1/b;\quad \tilde{c}=-\frac{c}{b(b+2c)};\quad \tilde{d}=-\frac{4}{h^2}\frac{d}{b+2c}$$

where

$$b=2\left[\frac{E_{\langle m+1\rangle}h_{\langle m+1\rangle}}{1+\nu_{\langle m+1\rangle}}+\sum_{r=1}^{m}\frac{E_{\langle r\rangle}(h_{\langle r\rangle}-h_{\langle r+1\rangle})}{1+\nu_{\langle r\rangle}}\right]$$

$$c=2\left[\frac{E_{\langle m-1\rangle}\nu_{\langle m+1\rangle}h_{\langle m+1\rangle}}{1-\nu^2_{\langle m-1\rangle}}+\sum_{r=1}^{m}\frac{E_{\langle r\rangle}\nu_{\langle r\rangle}(h_{\langle r\rangle}-h_{\langle r+1\rangle})}{1-\nu^2_{\langle r\rangle}}\right]$$

$$d=\frac{2}{3}\left[\frac{E_{\langle m+1\rangle}\nu'_{\langle m+1\rangle}G'_{\langle m+1\rangle}}{E'_{\langle m+1\rangle}(1-\nu_{\langle m+1\rangle})}h^3_{\langle m-1\rangle}+\sum_{r=1}^{m}\frac{E_{\langle r\rangle}\nu'_{\langle r\rangle}G'_{\langle r\rangle}}{E'_{\langle r\rangle}(1-\nu_{\langle r\rangle})}(h^3_{\langle r\rangle}-h^3_{\langle r+1\rangle})\right]$$

$$-2\left(\frac{h}{2}\right)^2\left[\frac{E_{\langle m+1\rangle}\nu'_{\langle m+1\rangle}G'_{\langle m+1\rangle}}{E'_{\langle m-1\rangle}(1-\nu_{\langle m+1\rangle})}h_{\langle m+1\rangle}+\sum_{r=1}^{m}\frac{E_{\langle r\rangle}\nu'_{\langle r\rangle}G'_{\langle r\rangle}}{E'_{\langle r\rangle}(1-\nu_{\langle r\rangle})}(h_{\langle r\rangle}-h_{\langle r+1\rangle})\right].$$